Frequency-Selective Single-Photon Detection Using a Double Quantum Dot

S. Gustavsson, M. Studer, R. Leturcq, T. Ihn, and K. Ensslin

Solid State Physics Laboratory, ETH Zürich, CH-8093 Zürich, Switzerland

D. C. Driscoll and A. C. Gossard

Materials Department, University of California, Santa Barbara, California 93106, USA

We use a double quantum dot as a frequency-tunable on-chip microwave detector to investigate the radiation from electron shot-noise in a near-by quantum point contact. The device is realized by monitoring the inelastic tunneling of electrons between the quantum dots due to photon absorption. The frequency of the absorbed radiation is set by the energy separation between the dots, which is easily tuned with gate voltages. Using time-resolved charge-detection techniques, we can directly relate the detection of a tunneling electron to the absorption of a single photon.

The interplay between quantum optics and mesoscopic physics opens up new horizons for investigating radiation produced in nanoscale conductors [1,2]. Microwave photons emitted from quantum conductors are predicted to show nonclassical behavior such as antibunching [3] and entanglement [4]. Experimental investigations of such systems require sensitive, high-bandwidth detectors operating at microwave frequency [5]. On-chip detection schemes, with the device and detector being strongly capacitively coupled, offer advantages in terms of sensitivity and large bandwidths. In previous work, the detection mechanism was implemented utilizing photon-assisted tunneling in a superconductor-insulator-superconductor junction [6,7] or in a single quantum dot (QD) [8].

Aguado and Kouwenhoven proposed to use a double quantum dot (DQD) as a frequency-tunable quantum noise detector [9]. The idea is sketched in Fig. 1(a), showing the energy levels of the DQD together with a quantum point contact (QPC) acting as a noise source. The DQD is operated with a fixed detuning δ between the electrochemical potentials of the left and right QD. If the system absorbs an energy $E = \delta$ from the environment, the electron in QD1 is excited to QD2. This electron may leave to the drain lead, a new electron enters from the source contact and the cycle can be repeated. The process induces a current flow through the system. Since the detuning δ may be varied continuously by applying appropriate gate voltages, the absorbtion energy is fully tunable.

The scheme is experimentally challenging, due to low current levels and fast relaxation processes between the QDs [10]. Here, we show that these problems can be overcome by using time-resolved charge-detection techniques to detect single electrons tunneling into and out of the DQD. Apart from giving higher sensitivity than conventional current measurement techniques, the method also allows us to directly relate a single-electron tunneling event to the absorbtion of a single photon. The system can thus be viewed as a frequency-selective single-photon detector for microwave energies. This, together with the

fact that the charge-detection methods allow precise determination of the device parameters, provide major advantages compared to other setups [2,5–8].

The sample [Fig. 1(b)] was fabricated by local oxidation [11] of a GaAs/$Al_{0.3}Ga_{0.7}$As heterostructure, containing a two-dimensional electron gas (2DEG) 34 nm below the surface. The structure consists of two QDs in series (marked by 1 and 2 in the figure) with a nearby QPC used as a charge detector (lower-right corner of the figure). The dots are coupled via two separate tunneling barriers, formed in the upper and lower arms between the QDs. For this experiment, only the upper arm was kept open, the lower one was pinched off. The gates T, B, L, and R are used to tune the height of the tunneling barriers, while gates $G1$ and $G2$ control the electrochemical potentials of the two QDs.
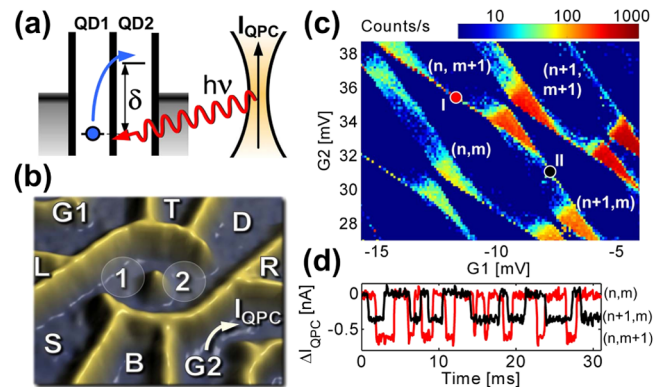

FIG. 1 (color online). (a) Schematic for operating a double quantum dot (DQD) as a high-frequency noise detector. The tunable level separation δ of the DQD allows frequency-selective detection. (b) The sample used in the measurement, with two QDs (marked by 1 and 2) and a nearby QPC. (c) Charge stability diagram of the DQD, measured by counting electrons entering the DQD. The numbers in brackets denote the charge population of the two QDs. (d) Typical traces of the detector signal, taken at point I (red) and II (black) in (c).

PHYSICAL REVIEW LETTERS

Because of electrostatic coupling between the QDs and the QPC, the conductance of the QPC is strongly influenced by the electron population of the QDs [12]. By applying a DC bias voltage to the QPC and continuously monitoring its conductance, electrons entering or leaving the QDs can be detected in real time [13–15]. The time resolution is limited by the noise of the amplifier and the capacitance of the cables, giving our setup a bandwidth of a few kHz.

The detection bandwidth puts an upper limit on the transition rates that can be measured [16]. In the experiment, we tune the tunneling rates between the QDs and the source or drain leads to be around 1 kHz, while the coupling t between the dots is kept at a relatively large value ($t = 32$ μeV, corresponding to 7.7 GHz). The large intradot coupling enhances the probability for the photon absorbtion process sketched in Fig. 1(a), but it also means that intradot transitions will occur on a time scale much faster than what is detectable.

Figure 1(c) shows a measurement of the count rate for electrons entering the DQD versus voltages on gates $G1$ and $G2$, with 600 μV bias applied between source (S) and drain (D). Resonant tunneling of electrons between the DQD and the source and drain contacts give rise to lines forming a hexagon pattern. At the crossing points of the lines, triangles with electron transport appear due to the applied bias. These features are well-known characteristics of DQDs and allow precise determination of the capacitances in the system [17]. The numbers in brackets denote the charge population of the two dots. Going from the region with population (n, m) to $(n, m + 1)$, resonant tunneling occurs as QD2 aligns with the drain lead [marked by point I in Fig. 1(c)]. Between regions (n, m) and $(n + 1, m)$, the tunneling occurs between QD1 and the source [point II]. Figure 1(d) displays time traces of the QPC current taken at point I (red) and point II (black), showing a few events where electrons enter and leave the DQD. Since the QPC is located closer to QD2 than to QD1, electron fluctuations in QD2 give a larger change in the QPC conductance than fluctuations in QD1. This enables us to do charge localization measurements [18,19]. By analyzing the charge distribution as a function of detuning δ, we extract the tunnel coupling energy between the QDs to be $t = 32$ μeV [18].

In the following, we present measurements taken with zero bias across the DQD. Figure 2(a) shows count rates close to the triple point where the $(n + 1, m)$, $(n, m + 1)$ and $(n + 1, m + 1)$ states are degenerate [see inset of Fig. 2(a)]. The arguments presented below are applicable also for the triple point between the (n, m), $(n + 1, m)$, $(n, m + 1)$ states, but for simplicity we consider only the first case. At the triple point [marked by a blue dot in Fig. 2(a)], the detuning δ is zero and both dots are aligned with the Fermi level of the leads. The two strong, bright lines emerging from this point come from resonant tunneling between the left (right) QD and the source (drain) lead. The height of the lines gives directly the strength of the tunnel
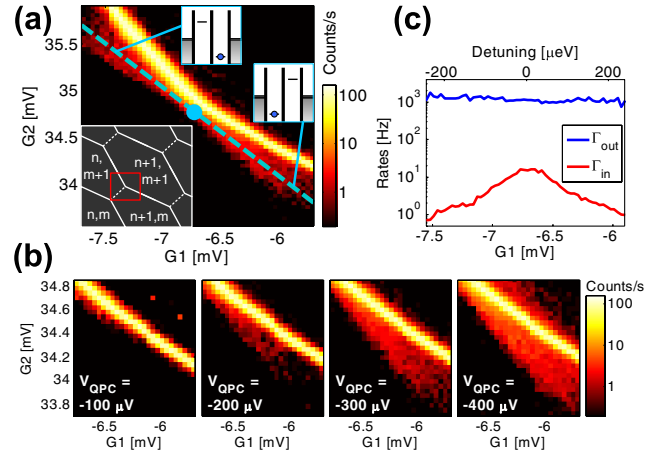

FIG. 2 (color online).   (a) Electron count rates for a small region close to a triple point (marked by a blue point). The inset shows a sketch of the surrounding hexagon pattern. The dashed line denotes the detuning axis, with zero detuning occurring at the triple point. The data was taken with $V_{QPC} = -300$ μV. (b) Enlargement of the lower-right region of (a), measured for different QPC bias voltages. (c) Rates for electron tunneling into and out of the DQD, measured along the dashed line in (a). Γ_{in} falls off rapidly with detuning, while Γ_{out} shows only minor variations.

couplings [14,20], and we find the rates to be $\Gamma_S = 1.2$ kHz and $\Gamma_D = 1.1$ kHz.

Along the blue dashed line in Fig. 2(a), there are triangle-shaped regions with low but nonzero count rates where tunneling is expected to be strongly suppressed due to Coulomb blockade. The DQD level arrangement inside the triangles is shown in the insets. Comparing with the sketch in Fig. 1(a), we see that both regions have DQD configurations favorable for noise detection. The dashed blue line connecting the triangles defines the detuning axis, with zero detuning occuring at the triple point. We take detuning to be negative in the upper-left part of the figure. In Fig. 2(b), the lower-right part of Fig. 2(a) was measured for four different QPC bias voltages. The resonant line stays the same in all four measurements, but the triangle becomes both larger and more prominent as the QPC bias is increased. This is a strong indication that the tunneling is due to absorbtion of energy from the QPC. The counts observed above the resonance line for $V_{QPC} = -400$ μV are due to electrons being excited from the ground state to the first excited state of QD1.

The time-resolved measurement technique allows the rates for electron tunneling into and out of the DQD to be determined separately [21]. Figure 2(c) shows the rates Γ_{in} and Γ_{out} measured along the dashed line of Fig. 2(a). The rate for tunneling out stays almost constant along the line, but Γ_{in} is maximum close to the triple point and falls of rapidly with increased detuning. This suggests that only the rate for electrons tunneling into the DQD is related to the absorbtion process. To explain the experimental findings we model the system using a rate-equation approach.

For a configuration around the triple point, the DQD may hold $(n + 1, m)$, $(n, m + 1)$ or $(n + 1, m + 1)$ electrons. We label the states L, R and 2 and draw the energy diagrams together with possible transitions in Fig. 3(a). The figure shows the case for positive detuning, with $\delta \gg k_B T$. Note that when the DQD holds two excess electrons, the energy levels are raised by the intradot charging energy, $E_{Ci} = 800$ μeV.

In Fig. 3(b) we sketch the time evolution of the system. The red curve shows the expected charge detector signal assuming a detector bandwidth much larger than the transitions rates. Starting in state L, the electron is trapped until it absorbs a photon and is excited to state R (with rate $\Gamma_{abs.}$). From here, the electron may either relax back to state L (rate $\Gamma_{rel.}$) or a new electron may enter QD1 from the source lead and put the system into state 2 (rate Γ_S). Finally, if the DQD ends up in state 2, the only possible transition is for the electron in the right dot to leave to the drain lead.

The relaxation rate for a similar DQD system has been measured to be $1/\Gamma_{rel.} = 16$ ns [22], which is much faster than the available measurement bandwidth. Therefore, the detector will not be able to register the transitions where the electron is repeatedly excited and relaxed between the dots. Only when a second electron enters from the source lead [transition marked by Γ_S in Figs. 3(a) and 3(b)], the DQD will be trapped in state 2 for a sufficiently long time ($\sim 1/\Gamma_D \sim 1$ ms) to allow detection. The measured time trace will only show two levels, as indicated by the dashed line in Fig. 3(b). Such a trace still allows extraction of the effective rates for electrons entering and leaving the DQD, $\Gamma_{in} = 1/\langle \tau_{in} \rangle$ and $\Gamma_{out} = 1/\langle \tau_{out} \rangle$. To relate Γ_{in}, Γ_{out} to the internal DQD transitions, we write down the Master equation for the occupation probabilities of the states:

$$\frac{d}{dt}\begin{bmatrix} p_L \\ p_R \\ p_2 \end{bmatrix} = \begin{bmatrix} -\Gamma_{abs.} & \Gamma_{rel.} & \Gamma_D \\ \Gamma_{abs.} & -(\Gamma_S + \Gamma_{rel.}) & 0 \\ 0 & \Gamma_S & -\Gamma_D \end{bmatrix} \begin{bmatrix} p_L \\ p_R \\ p_2 \end{bmatrix}. \quad (1)$$

Again, we assume positive detuning, with $\delta \gg k_B T$. The measured rates Γ_{in} for the limit $\Gamma_{rel.} \gg \Gamma_S, \Gamma_{abs.}$ is calculated from the steady-state solution of Eq. (1):
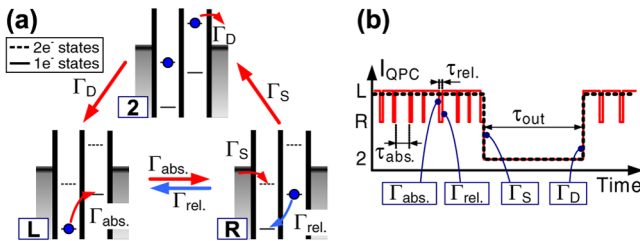

(a) ---- 2e⁻ states   —— 1e⁻ states

FIG. 3 (color online). (a) Energy level diagrams for the three states of the DQD. The labels L, R and 2 denote the excess charge population. The levels are raised by the intradot charging energy E_{Ci} when the DQD holds two excess electrons. (b) Schematic changes of the detector signal as electrons tunnel into, between and out of the DQD.

$$\Gamma_{in} = \Gamma_S p_R/(p_L + p_R) = \Gamma_S \Gamma_{abs.}/\Gamma_{rel.}. \quad (2)$$

The corresponding expression for negative detuning is found by interchanging Γ_S and Γ_D in Eq. (2). Assuming Γ_S and $\Gamma_{rel.}$ to be independent of detuning, a measurement of Γ_{in} gives directly the absorbtion spectrum of the DQD. The measurements cannot exclude that $\Gamma_{rel.}$ also varies with δ, but as we show below the model assuming $\Gamma_{rel.}$ independent of detuning fits the data well.

Equation (2) shows that the low-bandwidth detector can be used to measure the absorbtion spectrum, even in the presence of fast relaxation. Moreover, the detection of an electron entering the DQD implies that a quantum of energy was absorbed immediately before the electron was detected. The charge detector signal thus relates directly to the detection of a single photon. The efficiency of the detector is currently limited by the bandwidth of the charge detector. However, it should be possible to increase the bandwidth significantly by operating the QPC in a mode analogous to the radio-frequency single-electron transistor [23–25].

In the following, we use the DQD to quantitatively investigate the microwave radiation emitted from the nearby QPC. Figure 4(a) shows the measured Γ_{in} versus detuning and QPC bias. The data were taken along the dashed line of Fig. 2(a), with gate voltages converted into energy using lever arms extracted from finite-bias measurements. Because of the tunnel coupling t between the QDs, the energy level separation Δ_{12} of the DQD is given by $\Delta_{12} = \sqrt{4t^2 + \delta^2}$. The dashed lines in 4(a) show Δ_{12}, with $t = 32$ μeV. A striking feature is that there are no counts in regions with $|eV_{QPC}| < \Delta_{12}$. This originates from the fact that the voltage-biased QPC can only emit photons with energy $\hbar\omega \leq eV_{QPC}$ [5,8,9]. The result presents another strong evidence that the absorbed photons originate from the QPC.

To describe the results quantitatively, we consider the emission spectrum of a voltage-biased QPC with one conducting channel. In the low-temperature limit $k_B T \ll \hbar\omega$, the spectral noise density $S_I(\omega)$ for the emission side ($\omega > 0$) takes the form (see [9] for the full expression)

$$S_I(\omega) = \frac{4e^2}{h} D(1-D) \frac{eV_{QPC} - \hbar\omega}{1 - e^{-(eV_{QPC} - \hbar\omega)/k_B T}}, \quad (3)$$

where D is the transmission coefficient of the channel. Using the model of Ref. [9], we find the absorption rate of the DQD in the presence of the QPC:

$$\Gamma_{abs.} = \frac{4\pi e^2 k^2 t^2 Z_l^2}{h^2} \frac{S_I(\Delta_{12}/\hbar)}{\Delta_{12}^2}. \quad (4)$$

The constant k is the capacitive lever arm of the QPC on the DQD and Z_l is the zero-frequency impedance of the leads connecting the QPC to the voltage source. Equation (4) states how well fluctuations in the QPC couple to the DQD system.
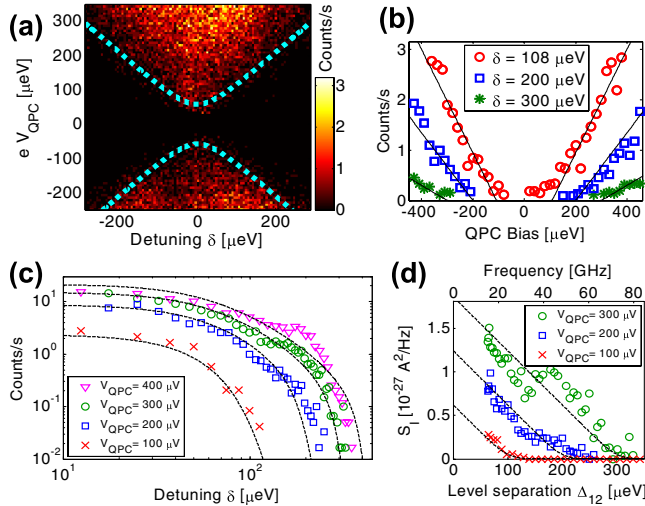
FIG. 4 (color online). Count rate measured versus detuning and QPC bias voltage. The dashed line shows the level separation for a two-level system, with $\Delta_{12} = \sqrt{4t^2 + \delta^2}$. There are only counts in the region where $|eV_{\mathrm{QPC}}| > \Delta_{12}$. (b) Count rate versus QPC bias for different values of detuning. The solid lines are guides to the eye. (c) DQD absorption spectrum, measured for different QPC bias. The dashed lines are the results of Eq. (4), with parameters given in the text. (d) Noise spectrum of the QPC, extracted from the data in (c). The dashed lines show spectra expected from Eq. (3).

Figure 4(b) shows the measured absorbtion rates versus V_{QPC}, taken for three different values of δ. As expected from Eqs. (3) and (4), the absorption rates increase linearly with bias voltage as soon as $|eV_{\mathrm{QPC}}| > \delta$. The different slopes for the three data sets are due to the $1/\Delta_{12}^2$-dependence in the relation between the emission spectrum and the absorption rate of Eq. (4). In Fig. 4(c), we present measurements of the absorption spectrum for fixed V_{QPC}. The rates decrease with increased detuning, with sharp cut-offs as $|\delta| > eV_{\mathrm{QPC}}$. In the region of small detuning, the absorption rates saturate as the DQD level separation Δ_{12} approaches the limit set by the tunnel coupling. The dashed lines show the combined results of Eqs. (2)–(4), with parameters $T = 0.1$ K, $Z_l = 0.7$ kΩ, $D = 0.5$, $t = 32$ μeV, $k = 0.15$, $\Gamma_S = 1.2$ kHz and $\Gamma_D = 1.1$ kHz. Using $\Gamma_{\mathrm{rel.}}$ as a fitting parameter, we find $1/\Gamma_{\mathrm{rel.}} = 5$ ns. This should be seen as a rough estimate of $\Gamma_{\mathrm{rel.}}$ due to uncertainties in Z_l, but it shows reasonable agreement with previously reported measurements [22]. The overall good agreement between the data and the electrostatic model of Eq. (4) supports the assumption that the interchange of energy between the QPC and the DQD is predominantly mediated by photons instead of phonons or plasmons.

The data for $V_{\mathrm{QPC}} = 400$ μV shows some irregularities compared to theory, especially at large positive detuning. We speculate that the deviations are due to excited states of the individual QDs, with excitation energies smaller than the detuning. In Fig. 4(d), we convert the detuning δ to

level separation Δ_{12} and use Eq. (4) to extract the noise spectrum S_I of the QPC. The linear dependence of the noise with respect to frequency corresponds well to the behavior expected from Eq. (3). Again, the deviations at $\Delta_{12} = 190$ μeV are probably due to an excited state in one of the QDs. The excited states are also visible in finite-bias spectroscopy, giving a single-level spacing of $\Delta E \approx 200$ μeV. This sets an upper bound on frequencies that can be detected with the detector. The frequency-range can be extended by using DQD in carbon nanotubes [26] or InAs nanowires [27,28], where the single-level spacing is significantly larger.

To summarize, we have shown that a DQD can be used as a frequency-selective detector for microwave radiation. Time-resolved charge-detection techniques allow single photons to be detected, giving the method a very high sensitivity. To prove the principle of the device we have investigated the high-frequency spectrum of radiation emitted from a voltage-biased QPC. The emission rate was found to increase linearly with applied bias, with a spectrum having a sharp cutoff for frequencies higher than the QPC bias.

[1] C. W. J. Beenakker and H. Schomerus, Phys. Rev. Lett. **86**, 700 (2001).
[2] J. Gabelli et al., Phys. Rev. Lett. **93**, 056801 (2004).
[3] C. W. J. Beenakker and H. Schomerus, Phys. Rev. Lett. **93**, 096801 (2004).
[4] C. Emary, B. Trauzettel, and C. W. J. Beenakker, Phys. Rev. Lett. **95**, 127401 (2005).
[5] E. Zakka-Bajjani et al., arXiv:0704.0907.
[6] R. Deblock et al., Science **301**, 203 (2003).
[7] E. Onac et al., Phys. Rev. Lett. **96**, 026803 (2006).
[8] E. Onac et al., Phys. Rev. Lett. **96**, 176601 (2006).
[9] R. Aguado and L. P. Kouwenhoven, Phys. Rev. Lett. **84**, 1986 (2000).
[10] V. S. Khrapai et al., Phys. Rev. Lett. **97**, 176803 (2006).
[11] A. Fuhrer et al., Superlattices Microstruct. **31**, 19 (2002).
[12] M. Field et al., Phys. Rev. Lett. **70**, 1311 (1993).
[13] T. Fujisawa et al., Appl. Phys. Lett. **84**, 2343 (2004).
[14] R. Schleser et al., Appl. Phys. Lett. **85**, 2005 (2004).
[15] L. M. K. Vandersypen et al., Appl. Phys. Lett. **85**, 4394 (2004).
[16] S. Gustavsson et al., Phys. Rev. B **75**, 075314 (2007).
[17] W. G. van der Wiel et al., Rev. Mod. Phys. **75**, 1 (2002).
[18] L. DiCarlo et al., Phys. Rev. Lett. **92**, 226801 (2004).
[19] T. Fujisawa et al., Science **312**, 1634 (2006).
[20] O. Naaman and J. Aumentado, Phys. Rev. Lett. **96**, 100201 (2006).
[21] S. Gustavsson et al., Phys. Rev. Lett. **96**, 076605 (2006).
[22] J. R. Petta et al., Phys. Rev. Lett. **93**, 186802 (2004).
[23] R. J. Schoelkopf et al., Science **280**, 1238 (1998).
[24] D. J. Reilly et al., Appl. Phys. Lett. **91**, 162101 (2007).
[25] T. Müller et al., AIP Conf. Proc. **893**, 1113 (2007).
[26] N. Mason, M. J. Biercuk, and C. M. Marcus, Science **303**, 655 (2004).
[27] C. Fasth et al., Nano Lett. **5**, 1487 (2005).
[28] A. Pfund et al., Appl. Phys. Lett. **89**, 252106 (2006).